Journal of Applied Physics

RESEARCH ARTICLE | FEBRUARY 12 2026

Non-reciprocal magnetoresistances in chiral tellurium

Shuchen Li ; Chang Niu ; Peide D. Ye ; Axel Hoffmann

Check for updates

J. Appl. Phys. 139, 063905 (2026)
https://doi.org/10.1063/5.0313356

View Online
Export Citation

Articles You May Be Interested In

Spin selectivity in elemental tellurium and other chiral materials

Appl. Phys. Lett. (December 2023)

Anisotropic lattice thermal conductivity in chiral tellurium from first principles

Appl. Phys. Lett. (December 2015)

Robust chiral spin transport in the antiferromagnetic iron oxide/heavy metal bilayers

Appl. Phys. Lett. (May 2024)

22 May 2026 16:59:46

AIP Advances
Why Publish With Us?
21DAYS average time to 1st decision
OVER 4 MILLION views in the last year
INCLUSIVE scope
Learn More
AIP Publishing

AIP Publishing

Journal of Applied Physics ARTICLE pubs.aip.org/aip/jap

Non-reciprocal magnetoresistances in chiral tellurium

Cite as: J. Appl. Phys. **139**, 063905 (2026); doi: 10.1063/5.0313356
Submitted: 21 November 2025 · Accepted: 15 January 2026 ·
Published Online: 12 February 2026

View Online Export Citation CrossMark

Shuchen Li,[1] Chang Niu,[2,3] Peide D. Ye,[2,3] and Axel Hoffmann[1,a)]

AFFILIATIONS

[1]Department of Materials Science and Engineering and Materials Research Laboratory, The Grainger College of Engineering, University of Illinois Urbana-Champaign, Urbana, Illinois 61801, USA
[2]Birck Nanotechnology Center, Purdue University, West Lafayette, Indiana 47907, USA
[3]Elmore Family School of Electrical and Computer Engineering, Purdue University, West Lafayette, Indiana 47907, USA

[a)]**Author to whom correspondence should be addressed:** axelh@illinois.edu

ABSTRACT

Materials with broken fundamental symmetries, such as chiral crystals, provide a rich playground for exploring unconventional spin-dependent transport phenomena. The interplay between a material's chirality, strong spin–orbit coupling, and charge currents can lead to complex non-reciprocal effects, where electrical resistance depends on the direction of current and magnetic fields. In this study, we systematically investigate the angular dependencies of magnetoresistance in single-crystalline chiral tellurium (Te). We observe distinct non-reciprocal magnetoresistances for magnetic fields applied along three orthogonal directions: parallel to the current along the chiral axis (**z**), in the sample plane but perpendicular to the current (**y**), and out of the sample plane (**x**). Through the detailed analysis of the chirality- and thickness dependence of the signals, we successfully disentangle multiple coexisting mechanisms. We conclude that the Edelstein effect, arising from the chiral structure's radial spin texture, is responsible for the non-reciprocity along the **z** axis. In contrast, the chirality-independent signal along the **y** axis is attributed to the Nernst effect, and the non-reciprocity along the **x** axis may originate from the orbital magnetization. These findings elucidate the complex interplay of spin, orbital, and thermal effects in Te, providing a complete picture of its non-reciprocal transport properties.

© 2026 Author(s). All article content, except where otherwise noted, is licensed under a Creative Commons Attribution (CC BY) license (https://creativecommons.org/licenses/by/4.0/). https://doi.org/10.1063/5.0313356

22 May 2026 16:59:46

I. INTRODUCTION

The breaking of fundamental symmetries in crystalline solids is a cornerstone for the discovery and manipulation of novel quantum phenomena.[1] In materials that lack a center of inversion, the interplay between the spin of an electron and its momentum, governed by strong spin–orbit coupling (SOC), gives rise to a host of unconventional transport effects that are forbidden in centrosymmetric systems.[2–6] One of the most fascinating of these is non-reciprocal charge transport, where the electrical resistance is not the same when the current direction is reversed. This effect serves as a powerful probe of symmetry breaking and has significant potential for applications in next-generation electronics.[7–9]

A primary mechanism for generating non-reciprocal transport is through the creation of a net spin polarization in the material. In systems with strong Rashba-type SOC, such as the polar semiconductor BiTeBr, an applied magnetic field can asymmetrically shift the spin-split Fermi surfaces, leading to a current-direction-dependent resistance, often termed unidirectional magnetoresistance (UMR) or bilinear magnetoelectric resistance.[10] This effect can be intuitively understood as the interplay between the external magnetic field and current-induced net spin polarizations that arise from the out-of-equilibrium shift of the spin-momentum-locked Fermi contours.[7,11] The magnitude of this non-reciprocity is directly tied to the strength of the underlying spin–orbit interaction, making it a valuable tool for quantifying spin-splitting. Moreover, its detailed angular dependence makes UMR an exceptionally sensitive probe of the complete three-dimensional spin texture, capable of revealing complex features beyond the standard Rashba model, such as the momentum-dependent out-of-plane spin components observed in $SrTiO_3$ based two-dimensional electron gas.[12] Distinct from this

© Author(s) 2026

spin-based mechanism, non-reciprocity can also arise from orbital degrees of freedom. In symmetry-breaking systems such as twisted bilayer graphene,[13] a net magnetization in the out-of-plane direction was observed due to a current-induced imbalance in the distribution of orbital magnetic moments. In chiral crystals, the structural helicity allows for the generation of a current-induced orbital magnetization.[14] While both effects are driven by the applied current and share the same phenomenological scaling ($V \propto I \cdot B$), they stem from fundamentally different angular momentum contributions—spin vs orbital—providing a unique opportunity to disentangle these quantum degrees of freedom through their distinct angular dependencies.

Tellurium (Te), an elemental material that has a chiral crystal structure with three tellurium atoms forming a spiral-shaped covalently bonded atomic chain in each unit cell, stands out as a compelling material for exploring non-reciprocal transport through the interplay among structural chirality and strong SOC.[15–17] The helicity of this atomic chain imparts a well-defined chirality, breaking both inversion and mirror symmetries. This unique crystallographic property, combined with a strong intrinsic SOC, lifts spin degeneracy and leads to a complex band structure with a radial spin texture at the Fermi surface. When a charge current is applied along the chiral axis, the Edelstein effect is predicted to induce a net spin polarization collinear with the current, with opposite polarities for right- and left-handed Te[18] as shown in Fig. 1(a), also making Te an ideal platform for investigating novel spintronic phenomena. This is a critical goal for developing next-generation, low-power electronic devices.[19–21] Moreover, with an application of an external magnetic field, non-reciprocal magnetoresistance has been found and reported in Te, while a comprehensive understanding of how structural chirality governs magnetotransport responses under various magnetic field orientations is still developing.[15,19,21–23] In this paper, we systematically investigate the non-reciprocal magnetoresistance in single-crystalline Te. We identify and disentangle three distinct non-reciprocal effects by analyzing their unique dependencies on crystal chirality, sample thickness, and magnetic field direction, attributing their origins to the Edelstein effect, the Nernst effect,[3,24] and the orbital magnetization,[14,25] respectively.

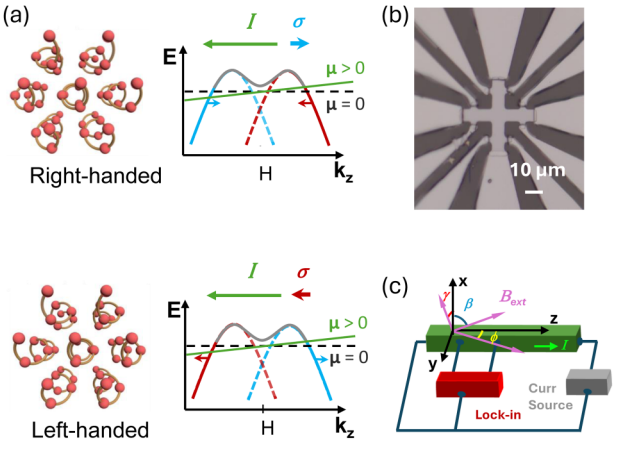

FIG. 1. (a)Diagrams showing left-handed and right-handed Te crystal structures and the corresponding spin polarizations due to the Edelstein effect. (b) Microscopic image of a fabricated Te device, with current channels both along and perpendicular to the chiral axis. (c) Schematics showing the measurement setup under various field scans.

II. MEASUREMENT

Single-crystalline Te flakes were grown by using the hydrothermal method,[21] and we used lithography and deposited Pt electrodes for transport measurements, in which a current is applied along the $+\mathbf{z}$, and $\mathbf{y}(\mathbf{x})$ direction is orthogonal to the current-direction in (out) of the device plane [Fig. 1(b)]. At the same time, a magnetic field B is applied in the $\mathbf{zy}(\mathbf{xz}, \mathbf{xy})$ plane, and we detected the longitudinal resistance using a lock-in amplifier at various angles $\phi(\beta, \gamma)$, where $\phi(\beta, \gamma)$ is the angle between B and $+\mathbf{z}(+\mathbf{x}, +\mathbf{x})$. In this paper, $\phi(\beta, \gamma) = 0°$ when B is parallel to $+\mathbf{z}(+\mathbf{x}, +\mathbf{x})$ and $\phi(\beta, \gamma) = 90°$ when B along the $+\mathbf{y}(+\mathbf{z}, +\mathbf{y})$ axis, as shown in Fig. 1(c).

We started our measurement by applying an ac current $I_0 \sin(\omega t)$ with $I_0 = 3 \times 10^{-4}$ A along the chiral axis of Te (R1) and collected the longitudinal first harmonic signal V_0^ω as we rotated the magnetic field in both the ϕ and β planes at 5 K. As shown in Figs. 2(a) and 2(d), we plot $\Delta V_0^\omega = V_0^\omega - V_{0,average}^\omega$ as a function of ϕ and β at $B = 2$ T, and we found Te has the largest magnetoresistance when B is out-of-plane along $\mathbf{x}$ and smallest when B is parallel with the chiral axis and the current direction.

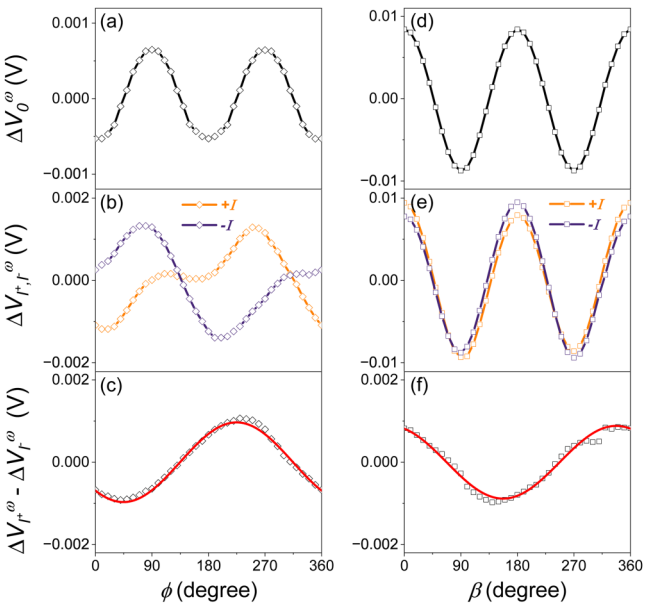

FIG. 2. (a) and (d) β and ϕ scans of mangetoresistance of Te with pure ac currents. (b) and (e) ϕ, β scans of Te with positive (orange) and negative (purple) dc offsets at 5 K. (c) and (f) Angular dependencies of $\Delta V_{I^+}^\omega - \Delta V_{I^-}^\omega$ to extract components with sine and cosine angular dependencies.

22 May 2026 16:59:46

© Author(s) 2026

We then applied a positive dc offset I_{dc} to the ac current, with $I = I_0\sin(\omega t) + I_{dc}$, and $I_0 = |I_{dc}| = 3 \times 10^{-4}$ A, and performed similar ϕ and β scans. Interestingly, as shown in Figs. 2(b) and 2(e), we found that the angular dependencies (orange curves) of $\Delta V^{\omega}_{I^+} = V^{\omega}_{I^+} - V^{\omega}_{I^+,average}$ were drastically changed with the application of a positive dc offset, and Te magnetoresistances were no longer even with the field, with clear non-reciprocal features appearing in both ϕ and β scans. Specifically, in ϕ scan, we found $V^{\omega}_{I^+}$ is smaller when B is parallel to the current direction ($\phi = 0°$) and larger when they are antiparallel ($\phi = 180°$). Surprisingly, we have also observed a difference in $\Delta V^{\omega}_{I^+}$ when $\phi = 90°$ and 270°, with a smaller $\Delta V^{\omega}_{I^+}$ at $\phi = 90°$. The two non-reciprocal behaviors of magnetoresistance in ϕ scan also appear in β scans at $\beta = 90°$ and 270°. Remarkably, we also observed another non-reciprocal behavior when the field is along **x** out-of-plane, as $\Delta V^{\omega}_{I^+}$ at $\beta = 0°$ and 180° is different. We then reversed the current direction by applying a negative I_{dc} and observed behaviors of $\Delta V^{\omega}_{I^-}$ also reversed [purple curves in Figs. 2(d) and 2(e)] as expected.

Based on our experimental observations and the general D_3 point group symmetry constraints, we generalized the electrical resistance of Te as

$$R(I,B) = R_0\left[1 + B^2(\delta_z\cos\phi\sin(\theta) + \delta_y\sin\theta\sin\phi + \delta_x\cos\theta)^2 + \eta I^2\right] + IB(\alpha_z\sin\theta\cos\phi + \alpha_y\sin\theta\sin\phi + \alpha_x\cos\phi), \quad (1)$$

where R_0, I, and B represent the resistance of Te at zero field, the current, and the external magnetic field, respectively. The coefficients δ_z, δ_y, and δ_x correspond to the normal magnetoresistances of Te when B is along **z**, **y**, and **x** that will cause R to either decrease or increase with the field and are independent of current. On the other hand, α_z, α_y, and α_x correspond to the sizes of the non-reciprocal effects in Te for B along **z**, **y**, and **x**, which are dependent on both B and I, rectifying Te magnetoresistances. η is the coefficient for thermal effect.

Thus, when we applied a dc offset with $I = I_0\sin(\omega t) + I_{dc}$, the resultant longitudinal first harmonic signal V^{ω} would also be modified (see the supplementary material), giving rise to the observed non-reciprocal effects. To exclude other contributions in Te, we calculated and plotted $\Delta V^{\omega}_{I^+} - \Delta V^{\omega}_{I^-}$ under the same field but opposite dc offsets in Figs. 2(c) and 2(f), and extracted $\alpha_z = -3.1 \pm 0.2\,\mathrm{k\Omega/(A\cdot T)}$, $\alpha_y = -3.6 \pm 0.2\,\mathrm{k\Omega/(A\cdot T)}$, and $\alpha_x = 3.8 \pm 0.2\,\mathrm{k\Omega/(A\cdot T)}$ by using Eq. (1) from cosine and sine components in the ϕ and β dependencies of ΔV^{ω} easily.

It is instructive to study also the non-linear second harmonic signal $V^{2\omega}$ proportional to the current, which also reflects the non-reciprocal effects and is independent of I_{dc}, and the analysis of it can be complementary to that of V^{ω}. Figures 3(a)–3(c) show the $\Delta V^{2\omega}_B$ of Te (R1) as a function of B_z, B_y, and B_x up to 9 and 2 T due to system geometry restrictions, with various ac amplitude I_0 at 5 K, where $\Delta V^{2\omega}_B = (V^{2\omega}(\pm B) - V^{2\omega}(\mp B))/2$ is the absolute change in the second harmonic signal. Clear linear relationships with all B_z, B_y, and B_x can be observed from all I_0, agreed well with Eq. (1), confirming three non-reciprocal behaviors observed in the first harmonic magnetoresistance measurements. Figure 3(d) shows $\Delta V^{2\omega}_B/(I_0B)$ as a function of I_0 for B_z (red), B_y (blue), and B_x (green), and the slopes are directly proportional to the sizes of α_z, α_y, and α_x. We calculated $\alpha_z = -3.2 \pm 0.1\,\mathrm{k\Omega/(A\cdot T)}$, $\alpha_y = -7 \pm 0.1\,\mathrm{k\Omega/(A\cdot T)}$, and $\alpha_x = 4.9 \pm 0.1\,\mathrm{k\Omega/(A\cdot T)}$, comparable to the results derived from the magnetoresistance measurements. Similarly, we measured $V^{2\omega}$ for Te (L1) as a function of I_0 and fields. Figures 3(e)–3(g) show $\Delta V^{2\omega}_B$ as a function of B_z, B_y,

22 May 2026 16:59:46

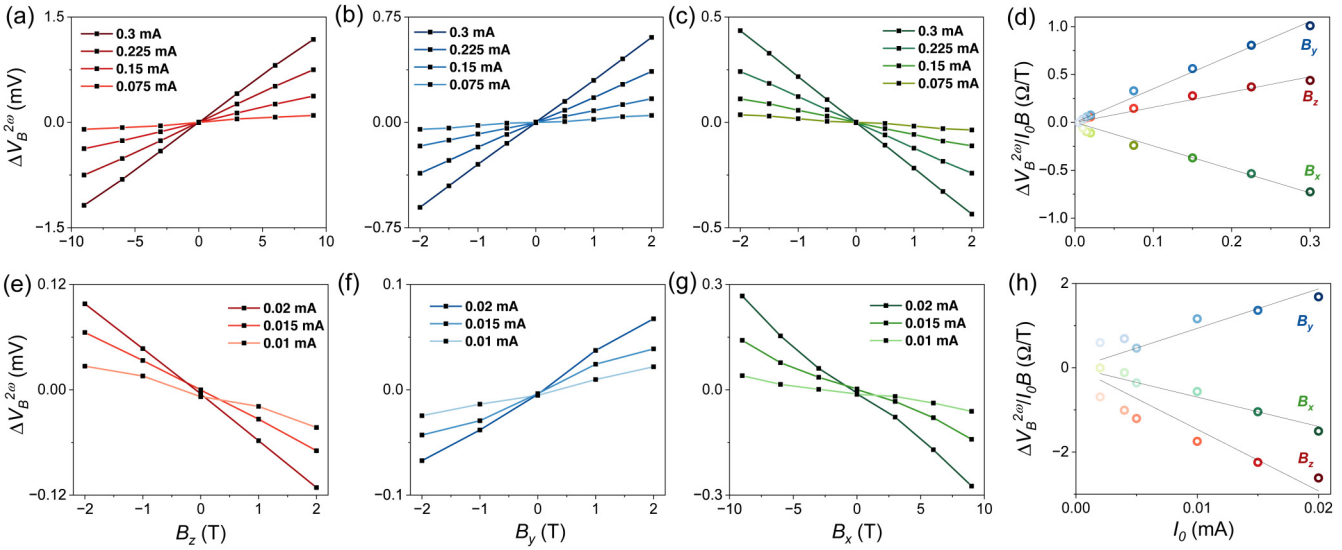

FIG. 3. (a)–(c) $\Delta V^{2\omega}_B$ under B_z, B_y, and B_x field sweep for Te(R1) at 5 K. (e)–(g) $\Delta V^{2\omega}_B$ under B_z, B_y, and B_x field sweep for Te(L1) at 5 K. (d) and (h) $\Delta V^{2\omega}_B/(I_0B)$ vs current for Te(R1) and (L1). Red, blue, and green dots correspond to $\Delta V^{2\omega}_B/(I_0B)$ at fields along B_z, B_y, and B_x at different current densities. The black solid lines are the linear fits for extracting α coefficients.

© Author(s) 2026

TABLE I. Resistances R_0 of different Te devices and extracted non-reciprocal effect coefficients α_z, α_y, α_x from second harmonic voltages. Right or left chirality is indicated by R and L with the device number followed.

Device	R_0 (kΩ)	α_z [kΩ/(A · T)]	α_y [kΩ/(A · T)]	α_x [kΩ/(A · T)]
L1	17.2	292.3 ± 26.4	−187.1 ± 19.2	139.3 ± 8.8
L2	14.9	172 ± 8.1	−126.5 ± 13.5	−119.2 ± 15.5
R1	1.2	−3.2 ± 0.1	−7 ± 0.1	4.9 ± 0.1
R2	1.3	−6.6 ± 0.9	−9.2 ± 0.2	−8.5 ± 0.6
L3	1.8	50.8 ± 8.3	−23.3 ± 3.0	
L4	1.7	44.1 ± 1.1	−38.1 ± 3.0	−6.3 ± 1.1
R3	2.0	−13.2 ± 2.7	−32 ± 4.2	
L5	1.6	6.7 ± 1.0	−19.7 ± 1.3	
R4	2.6	−14.9 ± 2.2	−45.7 ± 6.1	−51.1 ± 4.4
R5	16.2	−196 ± 12.9	−122 ± 8.8	207.5 ± 14.5

and B_x for different current densities along the chiral axis. Clearly, the slope of the B_z-dependency of $\Delta V_B^{2\omega}$ changed sign when Te chirality changed. However, the slope of B_y and B_x dependencies stayed the same. We then plot $\Delta V_B^{2\omega}/(I_0 B)$ as a function of I_0 in Fig. 3(h) and extract α_z, α_y, and α_x to be 292.3 ± 26.4 kΩ/(A · T), −187.1 ± 19.2 kΩ/(A · T), and 139.3 ± 8.8 kΩ/(A · T). We noticed a significant difference in the magnitudes of all coefficients between the two samples, which is likely related to their different resistances (1200 Ω vs 17 200 Ω), so we studied the thickness dependence of α_z, α_y, and α_x by performing the second harmonic measurements across a wide range of Te samples with various thicknesses. Table I shows the calculated coefficients together with the resistances of corresponding devices. We note that all devices were fabricated using a standardized lithography design with nominally identical channel dimensions. While minor variations in the aspect ratio (L/W) exist due to flake geometry, these are small compared to the wide range of flake thicknesses (spanning an order of magnitude). Consequently, the variation in zero-field resistance R_0 across samples serves as a robust proxy for the inverse thickness ($R_0 \propto 1/t$). First, we found α_z indicates a clear chirality-dependent origin with both positive and negative signs among the samples, while α_y is always negative in all the samples measured, suggesting a chirality-independent origin. We also noticed that the sign of α_x also varied across different Te samples, but did not tie to that of α_z, which means α_x could have opposite signs even if α_z had the same sign, for example, from devices 1 and 2, suggesting distinct physical origins for α_z and α_x. We then plotted the ratio between the absolute values of extracted α_z, α_y, and α_x and the corresponding device resistance R_0 as a function of R_0 in Fig. 4, which are similar for all three coefficients across different resistances, indicating bulk effect involved.

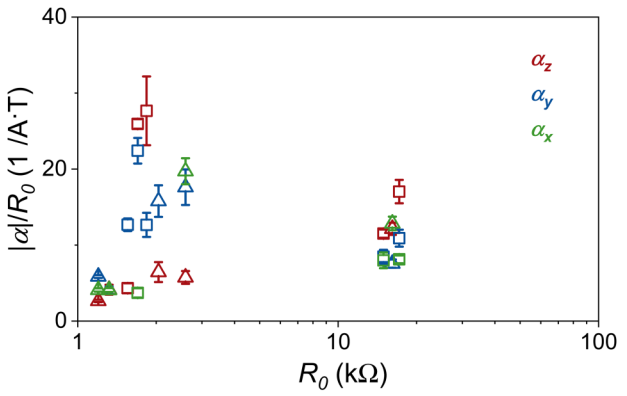

FIG. 4. Ratio of absolute values of extracted α_z, α_y, and α_x and the corresponding device resistance R_0 as a function of R_0. Squares and triangles represent the left and right handedness.

III. DISCUSSION

We would like to discuss possible origins behind the non-reciprocal magnetoresistances observed in Te, for fields along **z**, **y**, and **x** when current is along the chiral axis.

First, the non-reciprocal magnetoresistance along the chiral axis displayed a clear chirality-dependent behavior, which changed signs as we changed Te handedness, and we attributed that to the chirality-induced spin polarizations along the current directions due to the Edelstein effect and Te radial spin textures.[19]

However, the non-reciprocal magnetoresistances when B is along **y** that always had the same polarities regardless of the handedness, and the corresponding coefficient α_y is always negative for all the samples measured, strongly suggesting a chirality-independent origin behind, and we proposed the Nernst effect could explain the observations, that is, a thermal gradient ΔT generated out-of-plane could give rise to different magnetoresistances for $\pm B_y$, whose magnitude is proportional to $\Delta T \times B_y$. We note that thermally generated ΔT does not reverse when we reversed the DC bias, and α_y would always be negative.

Finally, we attribute the non-reciprocal magnetoresistance observed under an out-of-plane magnetic field ($B \parallel$ **x**) to the current-induced orbital magnetization. Unlike an ideal solenoid, the triangular helical crystal structure of Te generates not only a longitudinal moment (M_z) along the chiral axis[15] but also a significant transverse orbital magnetization (M_y) perpendicular to the chiral axis.[14] We note that in a bulk crystal preserving strict C_3 symmetry, these transverse moments would sum to zero due to the cancelation of equivalent radial directions. However, this macroscopic cancelation is likely lifted in our devices by the symmetry breaking at the interface or potentially by polar effects inherent to the 2D limit.[25] This extrinsic symmetry reduction allows the net transverse orbital moment—originating from the triangular helical structure—to manifest. Consequently, the interaction between this transverse moment M_y and the out-of-plane field (B_x) induces a rectification voltage $V_{orb,y} \propto M_y \times B_x$. Crucially, because M_y is fixed to the crystal lattice, its sign in the laboratory frame depends on the specific azimuthal orientation of the flake. We attribute the observed variability in the sign of α_x among samples of the same chirality to the random nature of device fabrication, where flakes may be deposited either "face-up" or "face-down" (corresponding to a 180° rotation about the **z** axis). Such a rotation reverses the transverse component M_y relative to the external field, flipping the

22 May 2026 16:59:46

© Author(s) 2026

sign of the measured non-reciprocity, whereas the chirality-dependent longitudinal response remains unaffected.

IV. CONCLUSION

In summary, we have systematically characterized the angular-dependent magnetoresistance in single-crystalline chiral Te flakes. Our measurements reveal three distinct non-reciprocal transport phenomena when a current is applied along the chiral axis. We have successfully disentangled their physical origins based on their unique dependencies on crystal chirality and magnetic field orientation. The chirality-dependent non-reciprocity along the transport direction is attributed to the Edelstein effect acting on the radial spin texture of Te's surface states. A second, chirality-independent effect is explained by the Nernst effect arising from a thermally generated gradient. Finally, a third non-reciprocity, observed with an out-of-plane field, is consistent with the influence of an intrinsic orbital magnetization. The pronounced thickness dependence of both the Edelstein effect and the orbital magnetization contributions indicates that while interfacial symmetry breaking is required to observe the net signal, the underlying mechanism is consistent with a bulk-driven effect arising from the helical bands, rather than being dominated solely by surface states. These findings not only provide a comprehensive picture of the complex interplay between charge, spin, and orbital degrees of freedom in a chiral conductor but also highlight the potential of tellurium for developing novel spintronic and orbitronic devices.

SUPPLEMENTARY MATERIAL

See the supplementary material for the detailed derivation of the first and second harmonic voltage responses in the presence of a DC current offset, as well as additional information regarding the experimental setup and data analysis.

ACKNOWLEDGMENTS

The authors would like to thank Paul Rutherford, Mandela Mehraeen, and Shulei Zhang (Case Western Reserve University) for their insightful discussions regarding the origins behind Te's non-reciprocal magnetoresistance behaviors, and Ruihao Liu (Tsinghua University) for initiating the discussion between the authors and fostering this collaborative work. Support for the magnetoresistance measurements, data analysis, and manuscript preparation was provided by the Air Force Office of Scientific Research (AFOSR) MURI program under Award No. FA9550-23-1-0311.

AUTHOR DECLARATIONS

Conflict of Interest

The authors have no conflicts to disclose.

Author Contributions

Shuchen Li: Data curation (equal); Formal analysis (equal); Software (equal); Validation (equal); Visualization (equal); Writing – original draft (equal); Writing – review & editing (equal). **Chang Niu:** Investigation (equal); Resources (equal); Validation (equal); Writing – review & editing (equal). **Peide D. Ye:** Resources (supporting); Supervision (supporting); Writing – review & editing (equal). **Axel Hoffmann:** Conceptualization (equal); Funding acquisition (equal); Investigation (equal); Project administration (equal); Supervision (equal); Validation (equal); Writing – review & editing (equal).

DATA AVAILABILITY

The data that support the findings of this study are available within the article and its supplementary material.

REFERENCES

[1]I. Žutić, J. Fabian, and S. Das Sarma, "Spintronics: Fundamentals and applications," Rev. Mod. Phys. **76**, 323–410 (2004).
[2]A. Manchon, H. C. Koo, J. Nitta, S. M. Frolov, and R. A. Duine, "New perspectives for Rashba spin–orbit coupling," Nat. Mater. **14**, 871–882 (2015).
[3]T. Kikkawa, K. Uchida, Y. Shiomi, Z. Qiu, D. Hou, D. Tian, H. Nakayama, X.-F. Jin, and E. Saitoh, "Longitudinal spin Seebeck effect free from the proximity Nernst effect," Phys. Rev. Lett. **110**, 067207 (2013).
[4]R. Klause, S. Li, Y. Xiao, J. Gibbons, H.-C. Ni, J. Qian, J.-M. Zuo, E. E. Fullerton, and A. Hoffmann, "Unconventional spin-orbit torques due to reduced crystal symmetries," IEEE Trans. Magn. **61**, 1–7 (2025).
[5]R. Klause, Y. Xiao, J. Gibbons, V. P. Amin, K. D. Belashchenko, D. Go, E. E. Fullerton, and A. Hoffmann, "Unconventional fieldlike spin torques in $CrPt_3$," Phys. Rev. Appl. **22**, 044043 (2024).
[6]S. Li, J. Gibbons, S. Chyczewski, Z. Liu, H.-C. Ni, J. Qian, J.-M. Zuo, J.-F. Zheng, W. Zhu, and A. Hoffmann, "Unconventional spin-orbit torques from sputtered $MoTe_2$ films," Phys. Rev. B **110**, 024426 (2024).
[7]P. He, S. S.-L. Zhang, D. Zhu, Y. Liu, Y. Wang, J. Yu, G. Vignale, and H. Yang, "Bilinear magnetoelectric resistance as a probe of three-dimensional spin texture in topological surface states," Nat. Phys. **14**, 495–499 (2018).
[8]Y. Tokura and N. Nagaosa, "Nonreciprocal responses from non-centrosymmetric quantum materials," Nat. Commun. **9**, 3740 (2018).
[9]M. Suárez-Rodríguez, F. de Juan, I. Souza, M. Gobbi, F. Casanova, and L. E. Hueso, "Nonlinear transport in non-centrosymmetric systems," Nat. Mater. **24**, 1005–1018 (2025).
[10]T. Ideue, K. Hamamoto, S. Koshikawa, M. Ezawa, S. Shimizu, Y. Kaneko, Y. Tokura, N. Nagaosa, and Y. Iwasa, "Bulk rectification effect in a polar semiconductor," Nat. Phys. **13**, 578–583 (2017).
[11]T. Guillet, C. Zucchetti, Q. Barbedienne, A. Marty, G. Isella, L. Cagnon, C. Vergnaud, H. Jaffrès, N. Reyren, J.-M. George, A. Fert, and M. Jamet, "Observation of large unidirectional Rashba magnetoresistance in Ge(111)," Phys. Rev. Lett. **124**, 027201 (2020).
[12]P. He, S. M. Walker, S. S.-L. Zhang, F. Y. Bruno, M. S. Bahramy, J. M. Lee, R. Ramaswamy, K. Cai, O. Heinonen, G. Vignale, F. Baumberger, and H. Yang, "Observation of out-of-plane spin texture in a $SrTiO_3(111)$ two-dimensional electron gas," Phys. Rev. Lett. **120**, 266802 (2018).
[13]W.-Y. He, D. Goldhaber-Gordon, and K. T. Law, "Giant orbital magnetoelectric effect and current-induced magnetization switching in twisted bilayer graphene," Nat. Commun. **11**, 1650 (2020).
[14]Z. Hua, C. Niu, S. Joy, P. Tan, G. Shi, H. Liu, J. Guo, D. Graf, P. Ye, C. Lewandowski, and P. Xiong, "Interplay of orbital and spin magnetization in trigonal tellurium," arXiv:2507.14292.
[15]T. Furukawa, Y. Watanabe, N. Ogasawara, K. Kobayashi, and T. Itou, "Current-induced magnetization caused by crystal chirality in nonmagnetic elemental tellurium," Phys. Rev. Res. **3**, 023111 (2021).
[16]M. Sakano, M. Hirayama, T. Takahashi, S. Akebi, M. Nakayama, K. Kuroda, K. Taguchi, T. Yoshikawa, K. Miyamoto, T. Okuda, K. Ono, H. Kumigashira, T. Ideue, Y. Iwasa, N. Mitsuishi, K. Ishizaka, S. Shin, T. Miyake,

22 May 2026 16:59:46

© Author(s) 2026

S. Murakami, T. Sasagawa, and T. Kondo, "Radial spin texture in elemental tellurium with chiral crystal structure," Phys. Rev. Lett. **124**, 136404 (2020).
[17]C. Niu, G. Qiu, Y. Wang, Z. Zhang, M. Si, W. Wu, and P. D. Ye, "Gate-tunable strong spin-orbit interaction in two-dimensional tellurium probed by weak antilocalization," Phys. Rev. B **101**, 205414 (2020).
[18]V. Edelstein, "Spin polarization of conduction electrons induced by electric current in two-dimensional asymmetric electron systems," Solid State Commun. **73**, 233–235 (1990).
[19]F. Calavalle, M. Suárez-Rodríguez, B. Martín-García, A. Johansson, D. C. Vaz, H. Yang, I. V. Maznichenko, S. Ostanin, A. Mateo-Alonso, A. Chuvilin, I. Mertig, M. Gobbi, F. Casanova, and L. E. Hueso, "Gate-tuneable and chirality-dependent charge-to-spin conversion in tellurium nanowires," Nat. Mater. **21**, 526–532 (2022).
[20]Q. Shao, P. Li, L. Liu, H. Yang, S. Fukami, A. Razavi, H. Wu, K. Wang, F. Freimuth, Y. Mokrousov, M. D. Stiles, S. Emori, A. Hoffmann, J. Åkerman, K. Roy, J.-P. Wang, S.-H. Yang, K. Garello, and W. Zhang, "Roadmap of spin–orbit torques," IEEE Trans. Magn. **57**, 1–39 (2021).
[21]C. Niu, S. Huang, N. Ghosh, P. Tan, M. Wang, W. Wu, X. Xu, and P. D. Ye, "Tunable circular photogalvanic and photovoltaic effect in 2D tellurium with different chirality," Nano Lett. **23**, 3599–3606 (2023). pMID: 37057864.
[22]M. Suárez-Rodríguez, B. Martín-García, F. Calavalle, S. S. Tsirkin, I. Souza, F. de Juan, A. Fert, M. Gobbi, L. E. Hueso, and F. Casanova, "Symmetry origin and microscopic mechanism of electrical magnetochiral anisotropy in tellurium," Phys. Rev. B **111**, 024405 (2025).
[23]B. Ma, M. Xie, L. Zhang, S. Liu, G. Ye, X. Yang, Y. Liu, F. Chu, Y. Liu, X. Zeng, X. Lu, and X. Wang, "Weyl node-participated magnetoresistance and nonreciprocal transport in two-dimensional tellurene nanostructures," ACS Appl. Nano Mater. **7**, 9012–9019 (2024).
[24]M. Weiler, M. Althammer, F. D. Czeschka, H. Huebl, M. S. Wagner, M. Opel, I.-M. Imort, G. Reiss, A. Thomas, R. Gross, and S. T. B. Goennenwein, "Local charge and spin currents in magnetothermal landscapes," Phys. Rev. Lett. **108**, 106602 (2012).
[25]P. Fontana, V. Velasco, C. Niu, P. D. Ye, P. V. Lopes, K. E. M. de Souza, M. V. O. Moutinho, C. Lewenkopf, and M. B. S. Neto, "Quantum geometry and the electric magnetochiral anisotropy in noncentrosymmetric polar media," Phys. Rev. Lett. **135**, 106602 (2025).

22 May 2026 16:59:46

© Author(s) 2026